Gas-phase Production of Monodisperse Ferroelectric Nanoparticles (<10 nm in Diameter)

Kwang Soo Seol*, Satoshi Tomita*, Kazuo Takeuchi*, Takahiro Katagiri*,**,
Takeshi Miyagawa*,**, and Yoshimichi Ohki**

*RIKEN, Hirosawa 2-1, Wako, Saitama 351-0198, Japan, seol@postman.riken.go.jp
**Waseda University, Shinjuku-ku, Tokyo 169-8555, Japan

ABSTRACT

Laser ablative technology was used to prepare monodisperse nanoparticles (<10 nm in diameter) of lead zirconate titanate (PZT) and strontium bismuth tantalate (SBT). Laser ablation of a ceramic target in oxygen ambience produced amorphous and irregularly-shaped nanoparticles of either PZT or SBT. A subsequent *on-line* thermal treatment performed on the nanoparticles dispersed in the gas phase brought about compaction and crystallization of the nanoparticles without additional particle growth. It was found that the amorphous PZT nanoparticles began to crystallize above 600 °C, and they became a perovskite structure at 900 °C. In contrast, the SBT nanoparticles began to crystallize at around 800 °C. The crystallized nanoparticles were then size-classified by a differential mobility analyzer to yield monodisperse, highly pure, and single-crystalline nanoparticles of PZT and SBT.

1. INTRODUCTION

Nanoparticles are of great interest in the field of materials science because they have unique size-dependent characteristics that are significantly different from those of bulk materials. For example, in semiconductor materials, the bandgap increases with a decrease in particle size due to the quantum confinement effect. Furthermore, ferromagnetic nanoparticles smaller than a critical size possess a single domain structure leading to magnetic properties superior to those of bulk materials.

The size effect has also been reported in ferroelectric nanoparticles, whereby ferroelectricity vanishes when the particles remain under a critical size.[1,2] Because this phenomenon causes a crucial problem for the development of nanometer-sized electronic devices using ferroelectric materials (e. g., nonvolatile ferroelectric random access memory (NVFRAM)), elucidation of the size effect is being urged. Although the size effect has been studied regarding nanoparticles of the complex ferroelectric metal oxides such as $BaTiO_3$[3-6] and $PbTiO_3$[2,7,8], substantial disagreement is still present about the critical size for each material.[8,9] This is due to the fact that the nanoparticles investigated in previous studies have tended to be much larger than the theoretically expected critical sizes[8] and have possessed a broad size distribution. Residual hydroxyl groups and carbon-related impurities in nanoparticles prepared by chemical methods also interfered with investigation on the intrinsic size effect.[3,6] Therefore, monodisperse and highly pure ferroelectric nanoparticles smaller than 10 nm are essential to achieve a better understanding of the size effect, because the effect becomes significant within the relevant size range.[8]

Synthesis of monodisperse ferroelectric nanoparticles with the relevant sizes using a sol-gel method is just beginning.[10,11] In the sol-gel process, high-temperature annealing (≥ 800 °C) is needed to completely eliminate hydroxyl groups and carbon-related impurities.[3] However, this leads to particle growth through coalescence and aggregation, which is fatal to synthesis of the nanoparticles smaller than 10 nm and free of the impurities.[3,6,10] From this point of view, it is still unclear that the ferroelectric nanoparticles synthesized by

the sol-gel process[10,11] are suitable for investigation on the size effect.

In comparison with the sol-gel method, it is advantageous to high purity that nanoparticles are prepared in clean gas ambience using sputtering, evaporation and condensation, or pulsed laser ablation (PLA). Monodisperse silicon nanoparticles smaller than 10 nm have recently been fabricated[12,13] by combining PLA with size-classification using a differential mobility analyzer[14]. PLA has also been demonstrated to be useful for the fabrication of thin films of ferroelectric oxides.[15,16] However, until now, PLA has not been attempted for the production of ferroelectric nanoparticles. Here, we report preparation of monodisperse nanoparticles (<10 nm in diameter) of lead zirconate titanate (PZT) and strontium bismuth tantalate (SBT), the most promising ferroelectric oxides in a NVFRAM[16], using PLA followed by both an *on-line* thermal treatment and size-classification.

2. EXPERIMENT

An experimental setup consists of in series connection of a laser ablation chamber, a charger, a furnace, and a very-low pressure differential mobility analyzer (VLPDMA) that has recently been developed by us[17,18] for particle size classification at Pa of a few hundred. PLA was performed by exposing either a PZT of SBT ceramic cylinder to a focused beam of either a second-harmonic generation or third-harmonic generation of Q-switched Nd:yttrium-aluminum-garnet (YAG) laser. The pulse width and frequency of the YAG laser were 6 ns and 10 Hz, respectively. The PLA was carried out with O_2 flows at a rate of 300 standard cm^3/min and at the following pressure: P_{O2} = 210-1300 Pa. The temperature T inside the furnace was controlled from about 20 °C to 1000 °C. Nanoparticles formed by PLA of PZT and SBT were transported by O_2 gases through a charger into a furnace in order to control the crystalline structure of the particles by an *on-line* thermal treatment. Nanoparticles were then introduced into a VLPDMA in order to classify the sizes of the charged particles. Size-selected nanoparticles were introduced into a Faraday-cup electrometer in order to measure the particle size distribution. The nanoparticles were collected on a carbon film supported by a copper grid used for transmission electron microscopy (TEM) analysis. The crystalline structure and the composition of the size-selected nanoparticles were investigated by selected area electron diffraction (SAD) and energy dispersive x-ray spectroscopy (EDX).

3. RESULTS

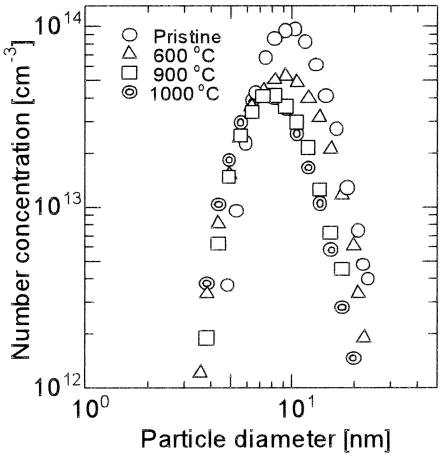

Fig. 1 Size distributions of PZT nanoparticles formed by laser ablation and thermal treatment at various temperatures.

Figure 1 shows the size distributions of PZT nanoparticles produced at P_{O2} = 400 Pa and treated at different temperatures. Both the particle concentration and average diameter values decreased with an increase in T. To analyze the effects of the *on-line* thermal treatment on particle morphology and the crystalline structure, nanoparticles size-classified at 15 nm were observed by TEM. Figure 2 shows the TEM images and the corresponding SAD patterns of the 9-nm nanoparticles treated at various T. At an O_2 flow rate of 300 standard cm^3/min and P_{O2} = 400 Pa, the thermal treatment time, i.e., the duration of residence of the nanoparticles in the furnace,

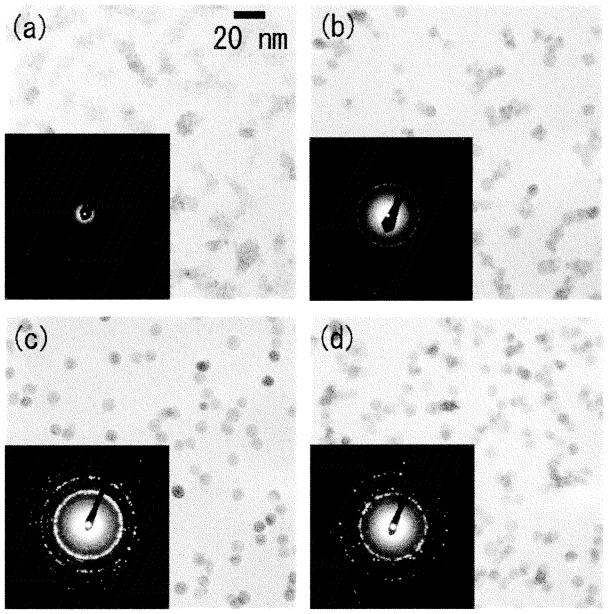

Fig. 2 TEM images and corresponding SAD patterns of pristine PZT nanoparticles (a) and PZT nanoparticles thermally treated at 600 °C (b), 900 °C (c), and 1000 °C (d).

was approximately 0.06 s. The pristine nanopartcles were irregularly shaped and contained spherical particulates 2-3 nm in diameter with the appearance similar to the frogs' eggs [see Fig. 2 (a)]. The SAD halo pattern shown in the inset of Fig. 2 (a) indicated that the pristine nanoparticles were primarily amorphous. Thermal treatments at $T \geq 600$ °C converted the irregularly shaped nanoparticles into spheres. An SAD pattern with Debye-Scherrer rings appeared in the nanoparticles at $T \geq 600$ °C. This indicated that the nanoparticles were primarily crystalline. These results suggest that compaction and crystallization of the amorphous nanoparticles began to occur at $T \geq 600$ °C. The observed decrease in the average particle diameter with an increase of T (see Fig. 1) was therefore due to the compaction and crystallization of the irregularly shaped nanoparticles brought out by the thermal treatment. The decrease in the particle concentration was most likely due to the thermophoretic deposition of nanoparticles at the cold end of the furnace.

The SAD pattern of the nanoparticles treated at T = 600 °C can be indexed to the pyrochlore phase of PZT.

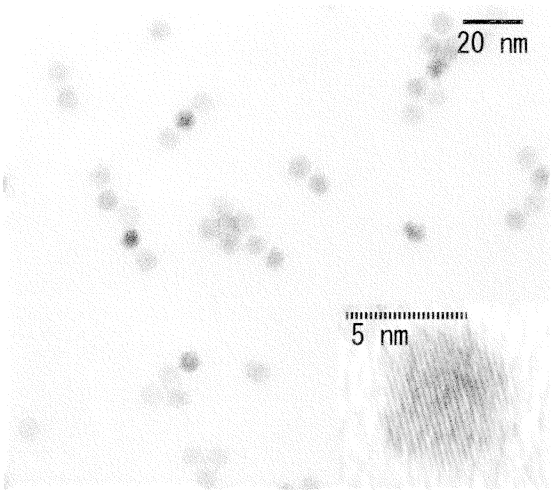

Fig. 3 A TEM image of PZT nanoparticles size-classified at a nominal 10 nm (lattice image inset).

The nanoparticles treated at T = 900 °C showed only diffraction rings originating from the perovskite phase of PZT. It was also found that the pyrochlore nanoparticles coexisted with the perovskite nanoparticles at T = 700 °C and 800 °C (Data not shown). In contrast, the SAD pattern of the nanoparticles treated at T = 1000 °C differed from either that of the pyrochlore or the perovskite structure. EDX measurement demonstrated that the nanoparticles treated at 900 and 1000 °C were composed of lead, zirconium, titanium, and oxygen, and that they did not contain any other impurities. It was also revealed that the nanoparticles treated at T = 900 °C were richer in lead than those at T =1000 °C. The plane distances were, in a large sequence, 0.36, 0.32, 0.29, 0.26, 0.22, 0.18, and 0.15 nm, which were obtained from the SAD pattern of the nanoparticles treated at T= 1000 °C. Except the planes with distances of 0.36 and 0.22 nm, distances of the other planes are close to those of the PZT pyrochlore.[19] This implies that the structure is probably similar to the PZT pyrochlore.[20]

The mean diameter and the geometric standard deviation were estimated to be 7 nm and 5.4 % respectively for the nanoparticles size-selected at a nominal 10 nm under the best conditions for DMA size classification, based on a TEM image (Fig. 3). Figure 3 (inset) shows a typical

high-resolution lattice image of a 7-nm diameter PZT nanoparticle. The high-resolution TEM image revealed that the nanoparticles were single-crystalline. From the size-distribution shown in Fig. 1, the smallest and largest PZT nanoparticles produced by the present conditions were estimated to be approximately 4 nm and 20 nm, respectively.

Similar particle morphology evolution was observed as a function of T in SBT. The pristine SBT nanoparticles formed by the laser ablation was primarily amorphous and irregularly shaped (Data not shown). The amorphous SBT nanoparticles were crystallized by the thermal treatment above 800 °C. The crystalline structure of the nanoparticles treated at 800 °C was fluorite. The crystalline structure of the particles treated at 1150 °C is still ambiguous because positions of the main diffraction peaks of fluorite, perovskite, and pyrochlore structures exists too closely to be separated by using electron beam diffraction method. It is however certain that the SBT nanoparticles treated at 1150 °C include the diffraction rings different from those due to both pyrochlore and fluorite structures. The crystallization temperature of the SBT nanoparticles higher than that of the PZT nanoparticles is consistent with the crystallization tendency of both materials reported in thin films.

4. CONCLUSIONS

The present method is widely applicable to other ferroelectric oxides as well as PZT and SBT. Using ceramic targets of various ferroelectric oxides and appropriate laser ablation conditions and T, we can apply this method to the fabrication of the nanoparticles of various ferroelectric oxides. Nanoparticles prepared in this manner will not only aid the investigation on the size effects of ferroelectric oxide nanoparticles, but preparation of such particles using the present method will also be useful for the fabrication of nanodevices using ferroelectric oxides.

REFERNCES

[1] K. Uchino, E. Sadanaga, and T. Hirose, J. Am. Ceram. Soc. 72, 1555 (1989).

[2] W. L. Zhong, Y. G. Wang, P. L. Zhang, and B. D. Qu, Phys. Rev. B 50, 698 (1994).

[3] M. H. Frey and D. A. Payne, Phys. Rev. B 54, 3158 (1996).

[4] S. Schlag and H. Eicke, Ferroelec. 173, 351 (1995).

[5] M. H. Frey and D. A. Payne, Appl. Phys. Lett. 63, 2753 (1993).

[6] S. Wada, H. Chikamori, T. Noma, and T. Suzuki, J. Mater. Sci. Lett. 19, 935 (2000).

[7] S. Chattopadhyay, P. Ayyub, V. R. Palkar, and M. Multani, Phys. Rev. B 52, 13177 (1995).

[8] B. Jiang, J. L. Peng, L. A. Bursill, and W. L. Zhong, J. Appl. Phys. 87, 3462 (2000).

[9] J. F. Scott, Integ. Ferroelec. 31, 139 (2000).

[10] C. Liu, B. Zou, A. J. Rondinone, and Z. J. Zhang, J. Am. Chem. Soc. 123, 4344 (2001).

[11] S. O'Brien, L. Brus, and C. B. Murray, J. Am. Chem. Soc. 123, 12085 (2001).

[12] R. P. Camata, H. A. Atwater, K. J. Vahala, and R. C. Flagan, Appl. Phys. Lett. 68, 3162 (1996).

[13] N. Suzuki, T. Makino, Y. Yamada, T. Yoshida, and T. Seto, App. Phys. Lett. 78, 2043 (2001).

[14] E. O. Knutson and K. T. Whitby, J. Aerosol Sci. 6, 443 (1975).

[15] *Pulsed Laser Deposition of Thin Films*, edited by D. B. Chrisey and G. K. Hubler (Wiley, New York, 1994).

[16] R. Ramesh, S. Aggarwal, and O. Auciello, Mater. Sci. Eng. R-Rep. 32, 191 (2001).

[17] K. S. Seol, Y. Tsutatani, R. P. Camata, J. Yabumoto, S. Isomura, Y. Okada, K. Okuyama, and K. Takeuchi, J. Aerosol Sci. 31, 1389 (2000).

[19] K. S. Seol, Y. Tsutatani, T. Fujimoto, Y. Okada, and H. Nagamoto, J. Vac. Sci. Technol. B 19, 1998 (2001).

[20] C. K. Kwok and S. B. Desu, Appl. Phys. Lett. 60, 1430 (1992).

[21] D. Kaewchinda, T. Chairaungsri, M. Naksata, S. J. Milne, and R. Brydson, J. Eur. Ceram. Soc. 20, 1277 (2000).